Asian Journal of Chemistry; Vol. 36, No. 2 (2024), 498-504

ASIAN JOURNAL OF CHEMISTRY

https://doi.org/10.14233/ajchem.2024.31064

Photocatalytic Degradation of Toxic Textile Dyes by Biosynthesized Silver Nanoparticles Synthesized from *Strobilanthes hamiltoniana* Leaf Extract

J. GANGWAR and K.S. JOSEPH*

Department of Life Sciences, Christ University, Bangalore-560029, India

*Corresponding author: E-mail: joseph.ks@christuniversity.in

Received: 16 December 2023; *Accepted*: 18 January 2024; *Published online*: 31 January 2024; AJC-21539

Biocompatible nanoparticle synthesis from *Strobilanthes hamiltoniana* leaf extracts is an ecologically friendly, cost-effective and long-lasting technique for wastewater treatment, particularly for textile dye degradation. *S. hamiltoniana* mediated silver nanoparticles (SH-Ag NPs) showed a maximum absorbance of 432 nm. Based on the FESEM analysis, the SH-Ag NPs were usually spherical with an average diameter of nm. The FTIR analyses revealed the significance of functional groups in the formation of SH-Ag NPs. Degradation and rate of degradation for textile dyes after 320 min, SH-Ag NPs displayed 88.4%, 79.49%, 0.0059 min^{-1} and 0.00495 min^{-1} for reactive blue 220 (RB-220) and reactive blue 222A (RB-222A) dyes. The phytotoxicity study of SH-Ag NPs treated dye solutions demonstrated a significant decrease in inhibitory efficiency when compared to dye effluents. The biosynthesized SH-Ag NPs could represent a viable catalyst alternative for treating textile dye degradation both before and after it enters aquatic environments.

Keywords: Photocatalytic degradation, Reactive blue dyes, Silver nanoparticles, Water pollution, Phytotoxicity.

INTRODUCTION

The improper disposal and discharge of textile dyes into bodies of water results in severe pollution, changing aquatic ecosystems and endangering human health. These hues typically include hazardous substances that, over time, affect aquatic life and groundwater supplies. Blue reactive dyes are harmful to both the environment and human health. When these dyes are discharged into bodies of water, they leak harmful compounds, causing aquatic ecosystems to change and groundwater to become contaminated [1]. Their persistent existence causes long-term harm to the aquatic life by reducing oxygen levels. Human exposure to these dyes has also been linked to skin rashes, allergies and maybe even cancerous effects. Inhaling or eating dye particles can be hazardous to one's respiratory and digestive systems, because they do not stick to clothing throughout the colouring process [2]. Blue reactive dyes have a harmful influence on water bodies, raising environmental problems. Their discharge disrupts aquatic environments by obstructing sunlight, reducing oxygen levels and interfering with photosynthesis. This harms fish and other aquatic animals, leading to an imbalance in food chains. Moreover, the longevity of dyes in water prevents natural degradation and constitutes a long-term contamination danger. Furthermore, these hues typically include harmful compounds that, if ingested, can enter the food chain and harm human health [3].

Various chemical and physical processes such as coagulation, flocculation and oxidation are widely used in traditional procedures for degrading the textile dyes. While these methods are effective, but they can produce secondary pollutants and consume a lot of energy and resources. Green-synthesized nanoparticles, on the other hand, are a more environmental friendly solution. Under more benign conditions, these nanoparticles, which are usually derived from biological sources such as plants, have excellent catalytic abilities for dye degradation [4]. Their distinct features, such as large surface area and catalytic activity, allow for effective dye degradation. Green synthesis techniques also include ecological friendly components, reducing the environmental effect. Despite the widespread use of traditional procedures, the integration of green-synthesized nanoparticles offers a potentially ecologically benign and effective option for textile dye degradation [5].

Biosynthesized nanoparticles have several benefits in the degradation of textile dyes. They are made with eco-friendly

procedures and biocompatible materials, lowering their environmental effect. Their unique characteristics, including as huge surface area and reactivity, allow for effective dye degradation. Green synthesis nanoparticles are also exceedingly stable, easily recovered and reusable, which reduces waste generation. Furthermore, these nanoparticles have the potential to target a wide range of dye types while also performing well in a number of operational conditions [6]. Because of their long term durability and efficacy in textile dye degradation, they are a viable option for reducing water pollution and encouraging ecologically friendly practices in the textile industries [7]. *Strobilanthes hamiltoniana*, often known as Chinese rain bell, is a member of the Acanthaceae family. Flavonoids, polyphenols, terpenoids, phenolic compounds and phytosterols are found in the leaves of *S. hamiltoniana*. These extracts exhibit antibacterial, antioxidant, antifungal, antioxidant, anticancer and anthelmintic effects [8].

In this study, a novel approach involves the use of *S. hamiltoniana* to biosynthesize Ag NPs (SH-Ag NPs) for textile dye degradation, namely reactive blue-220 (RB-220) and reactive blue-222A (RB-222A) dyes. The study focuses on the effective breakdown of these specific textile dyes by the utilization of the unique features of Ag NPs synthesized using environmental friendly procedures. The phytotoxicity analysis on the deteriorated dye were also performed to assess the harmful effects of the degraded substances.

EXPERIMENTAL

Silver nitrate was procured from Himedia laboratories for this study. The reactive blue dyes (RB-220 and RB-222A) were sourced from Jetpur textile industry, Rajkot, India. *Strobilanthes hamiltoniana* was identified and procured from Foundation for Revitalisation of Local Health Traditions (FRLHT), Bangalore, India.

Preparation of plant extract: Fresh picked leaves (5 g) of *Strobilanthes hamiltoniana* plants were carefully collected and rinsed thoroughly with distilled water to eliminate contaminants. The leaves were dried in a oven at 30 ºC and then the plant material was heated in 200 mL of distilled water using a reflux setup at 60 ºC. The heating process was repeated until the solution turns a brown colour. After obtaining the desired brown colored extract, it was allowed to settle to room temperature prior to filtration through Whatman filter paper No. 1 [9].

Biosynthesis of Ag NPs: The solution was diluted by adding distilled water, resulting in a doubling of its volume to 40 mL. Subsequently, 20 mL of $AgNO_3$ solution (0.03 M) was introduced into the solution. For around 10 min, this mixture was gradually warmed on a reflux setup until a significant brownish black precipitate appear. Subsequently, it was allowed to cool at the ambient temperature, so ensuring the continuous progression of the nanoparticle formation. The resulting silver nanoparticles were then collected using centrifugation at 150,000 rpm for 10 min. The nanoparticles were then rinsed with distilled water to eliminate any leftover components [9].

Characterization: The characteristics of biosynthesized nanoparticles were analyzed using several characterization techniques. The UV-Vis spectroscopy was used to analyze optical characteristics such as absorbance and bandgap using a UV-vis spectrophotometer (UV-1800, Shimadzu, Japan). To detect functional groups and chemical bonds in nanoparticles. The surface functional groups of Ag NPs were analyzed using FTIR technique (IR spirit-L, Shimadzu, Japan). The samples were directly placed on the sample holder, pressed and scanned in the frequency range of 4000-400 cm^{-1}. The crystalline structure and phase composition of biosynthesized nanoparticles were determined by X-ray diffraction (XRD) (Miniflex, Rigaku, Japan), with results obtained at 20-80º using Cu $K\alpha$ radiations at a wavelength of 1.541 Å. To analyze the size, shape and morphology of silver nanoparticles, TEM and FESEM (Carl Zeiss Model Supra 55) techniques can be utilized. The images were generated using the ImageJ program (version 1.53k).

Photocatalytic degradation of reactive blue textile dyes: The evaluation of photocatalytic degradation involved the utilization of azo dyes RB-220 and RB-222A, which are often employed in the textile industry. In distilled water, biosynthesized Ag NPs (1 mg/mL) were mixed with 1 ppm of RB-220 and RB-222A dyes. After being kept in dark for 10-15 min, the mixture was exposed to UV light in a photoreactor. An UV-visible spectrophotometer recorded absorbance over the 200-800 nm wavelength range at time intervals of 0, 10, 20, 40, 80, 160 and 320 min. The RB-220 and RB-222A dyes have absorbance maxima at 665 and 600 nm, respectively. The following equation was used to calculate the dye degradation effectiveness of the SH-Ag NPs.

$$\text{Degradation (\%)} = \frac{A_o - A_t}{A_o} \times 100$$

Phytotoxicity studies: A sprouting experiment was conducted to assess the potential adverse effects of *V. radiata* seeds. In this experiment, 10 seeds were planted in separate petri dishes, each with a 1 cm spacing between them. These seeds were subsequently exposed to a variety of solutions, including dye solutions, both treated and untreated, as well as nanoparticle solutions. The experiment analyzed the proportion of seedlings that germinated successfully after a 7 day treatment period, as well as the influence of toxicity on both shoot and root length [10].

$$\text{Germination (\%)} = \frac{\text{Seeds germinated}}{\text{Seeds placed for germination}} \times 100$$

The brine shrimp lethality experiment with *Artemia salina* was conducted using reported methods, with slight modifications. The eggs were incubated in artificial seawater (36 g of non-iodized salt dissolved in 1 L of deionized water) to hatch nauplii. These nauplii were then allowed to grow for 24 h at room temperature while exposed to both treated and untreated dye solutions as well as SH-Ag NPs. To determine the mortality rate (MR), the number of dead nauplii was counted and then calculated using the following eqn. [11]:

$$\text{Mortality (\%)} = \frac{\text{No. of dead nauplii}}{\text{Initial alive nauplii}} \times 100$$

RESULTS AND DISCUSSION

UV-Visible studies: The presence of phytochemicals in the plants acted as reducing agents and stabilizes silver ions

to silver during the synthesis of biogenic nanoparticles. After the addition of *S. hamiltoniana* leaves extract to silver nitrate, the colour of solution changed from light brown to brownish-black, suggesting the confirmed formation of SH-Ag NPs. Fig. 1 shows a prominent peak at 432 nm, which is well within 350-450 nm range as reported by earlier researchers who synthesized AgNPs from *Strobilanthes flaccidifolius* leaf extract [9] and andean blackberry fruit extract [12].

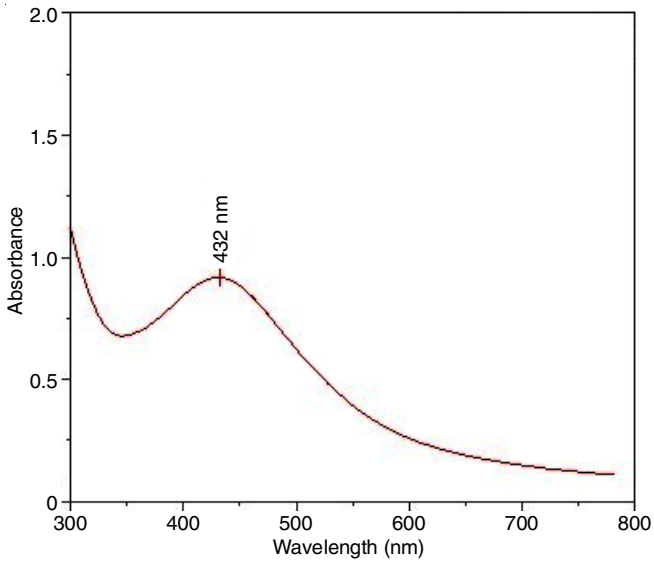

Fig. 1. UV-Vis spectrum of biosynthesized silver nanoparticles

XRD studies: The X-ray diffraction (XRD) patterns revealed the crystalline structure of SH-Ag NPs by distinct diffraction peaks. Specifically, the peaks were observed at 2θ values of 38.18º, 46.13º, 64.49º, 74.43º and 76.73º, corresponding to the crystalline phases of Ag NPs with indices [111], [002], [022] and [113], respectively (Fig. 2). By applying the Debye-Scherrer's equation, the average diameter of the biosynthesized nanoparticles was found to be 20.60 nm. The observed peaks corresponded with the JCPDS file no. 98-005-0882 [13].

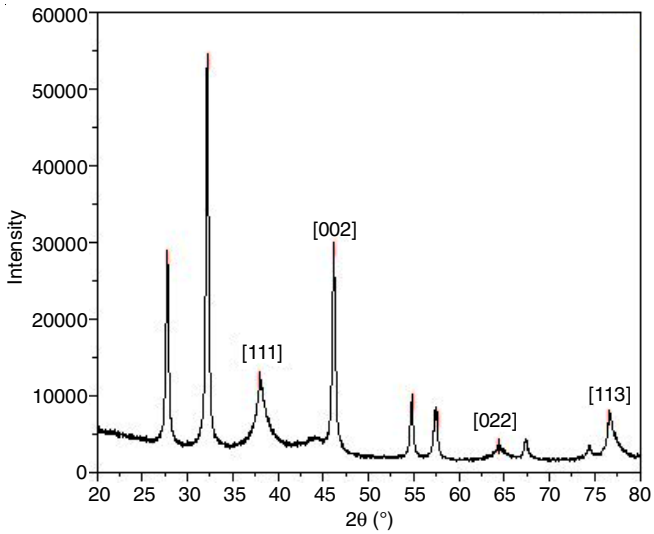

Fig. 2. XRD pattern of biosynthesized silver nanoparticles

FTIR studies: FTIR analysis was used to identify the silver bond formation and phytochemicals involved in biosynthesized Ag NPs. Peak absorbance values for -OH stretching vibrations were 3762.12, 3309.10, 2984.55, 2873.98 and 2030.65 cm^{-1}. Whereas the C-C stretching, C-H bending and C-N stretching were ascribed to the absorption peaks at 1890.80, 1489.16, 1352.89, 1286.54 and 840.68 cm^{-1}, respectively. The C-N stretching vibration confirmed the presence of alkaloid secondary metabolites. Similarly, the presence of saponins and flavonoids were characterized by the vibrations of -OH stretching, C-C stretching and C-H bending. The conversion of Ag^{+} ions into Ag NPs was facilitated by the secondary metabolites extracted from plants. When SH-Ag NPs are formed, a vibrational peak at 598.47 cm^{-1} is observed to Ag NPs bonding with sulfur group present in the extract [14] (Fig. 3).

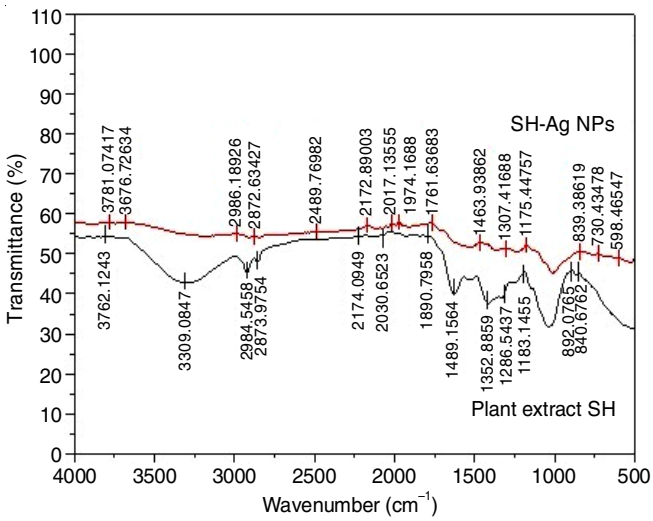

Fig. 3. FTIR spectra of biosynthesized silver nanoparticles and plant extract

FESEM studies: FESEM images at various magnifications were used to evaluate the morphology and sizes of the biosynthesized SH-Ag NPs as shown in Fig. 4a. These images demonstrated a spherical shape and agglomerated nanoparticle dispersion. The micrograph showed that nanoparticle polarity, surface characteristics, synergistic interactions and electrostatic attraction occured due to the Ag NP aggregation [9]. The average diameter of the SH-Ag NPs was measured to be 86.46 nm. A strong peak in the EDX spectra of the SH-Ag NPs (Fig. 4b) confirmed the biosynthesis of pure SH-Ag NPs. The spectra revealed that atom percentage for silver was the most significant element, accounting for 92.18% of the total, followed by carbon (7.28%) indicating the biosynthesis of pure Ag NPs.

TEM studies: The TEM images of silver show spherical particles, which is similar to the SEM findings. The majority of the Ag NPs are spherical with an average diameter of 15.41 nm (Fig. 5a). The SAED pattern indicated that the biosynthesized Ag diffraction rings exhibited Debye-Scherrer's values [111], [002], [022] and [222], respectively (Fig. 5b). The size of the particles detected by TEM appears to be similar to the size determined by the XRD pattern. Skiba *et al.* [15] synthesized Ag NPs in the presence of polysaccharide and observed a similar TEM pattern.

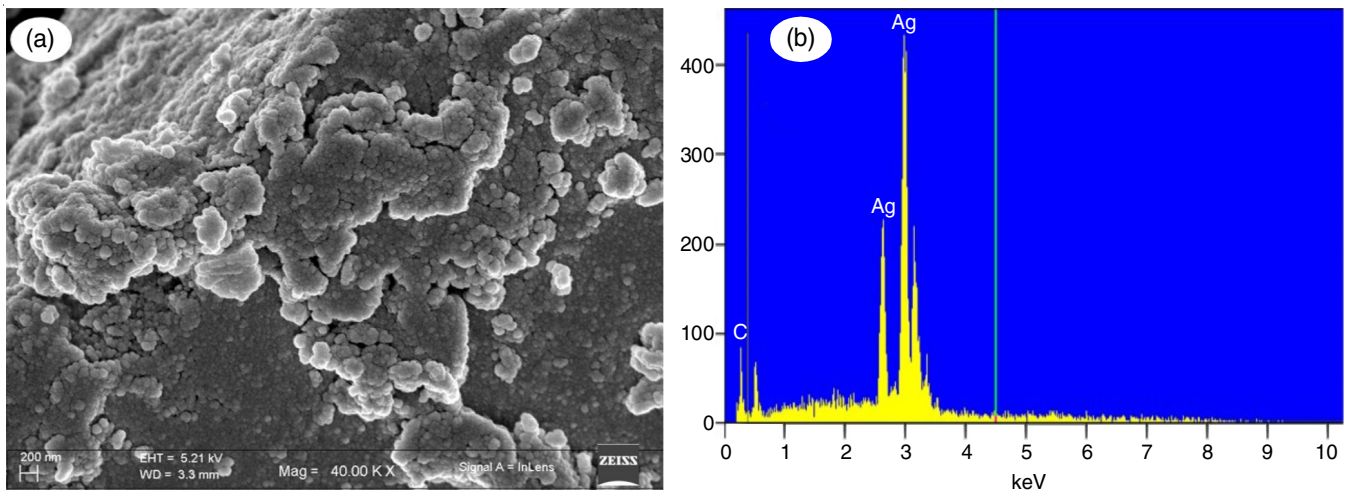

Fig. 4. SEM images of biosynthesized silver nanoparticles (SH-Ag NPs) at different magnifications (a) 200 nm and (b) EDX spectral composition

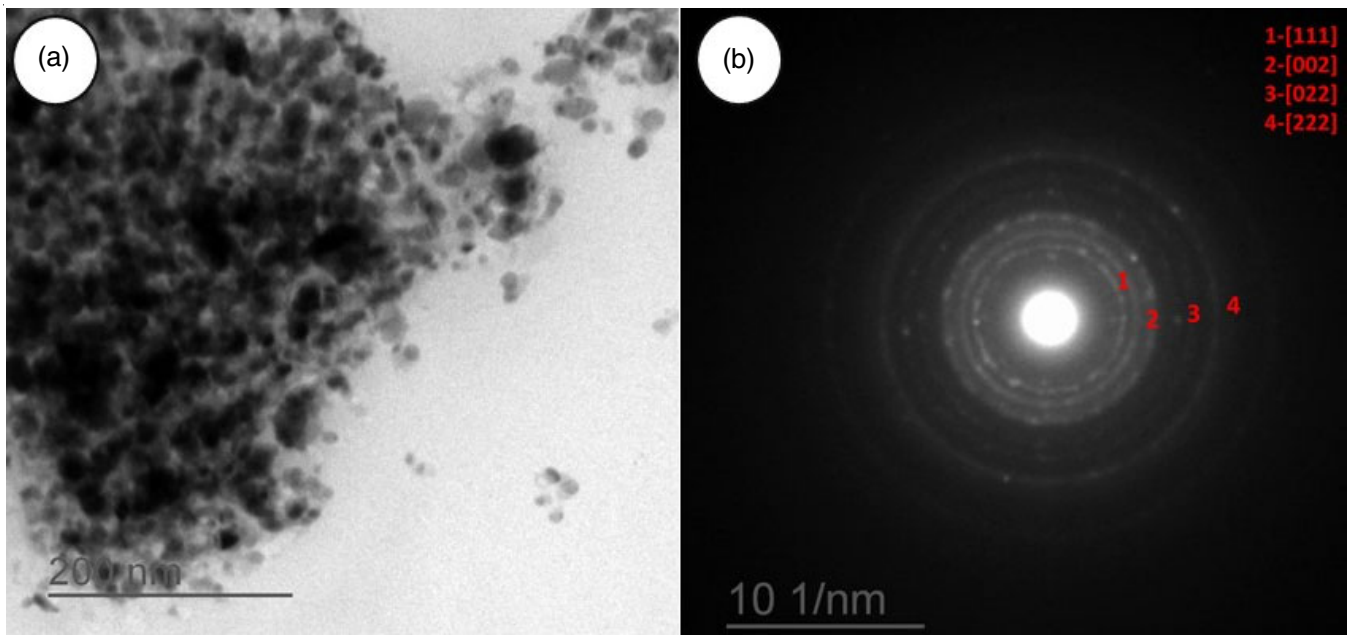

Fig. 5. TEM analysis (a) 200 nm and (b) SAED pattern of biosynthesized silver nanoparticles (SH-Ag NPs)

Photocatalytic degradation of textile dyes: The degrading efficiency of biosynthesized SH-Ag NPs was evaluated using the RB-220 and RB-222A dyes under UV irradiation. Furthermore, dye photo-degradation was assessed using the UV-vis spectra of the reaction mixture at 665 nm and 600 nm for RB-220 and RB-222A, respectively. Fig. 6 demonstrates the dependent-on-time breakdown of the RB-220 and RB-222A dyes. The absorbance of RB-220 dye decreased with time from 0 to 320 min, suggesting a progressive drop in dye concentration and degradation efficiency of 88.4% and 79.49% after 320 min, respectively (Fig. 6a-b). The linear relationship observed between $\ln(A_t/A_o)$ and reaction time (good correlation $R^2 > 0.95$) shows that the reaction followed pseudo-first-order kinetics [16]. The first-order rate constant (k) was calculated using the slope of the fitted linear regression plot and can be represented by the following eqn. 2:

$$\ln\left(\frac{A_t}{A_o}\right) = -kt$$

where A_o and A_t represent the dyes time-dependent concentrations, respectively; k is a rate constant; and t represents the time intervals. The rate constant (k) value of the SB-ZnO NPs used to degrade RB-220 and RB-222A was found to be 0.0059 min^{-1} and 0.00495 min^{-1}, respectively (Fig. 6c-d).

Proposed mechanism: When exposed to UV light, Ag NPs nanoparticles absorb photons and form electron-hole pairs on their surfaces. The photocatalytic process in which eventually breaks down the reactive dye molecules in the solution. Highly reactive oxygen species (ROS), such as superoxide radicals ($O_2^{\bullet-}$) and hydroxyl radicals ($^{\bullet}OH$) are produced by the interaction of excited electrons in the nanoparticle conduction band with oxygen molecules in the surrounding environment.

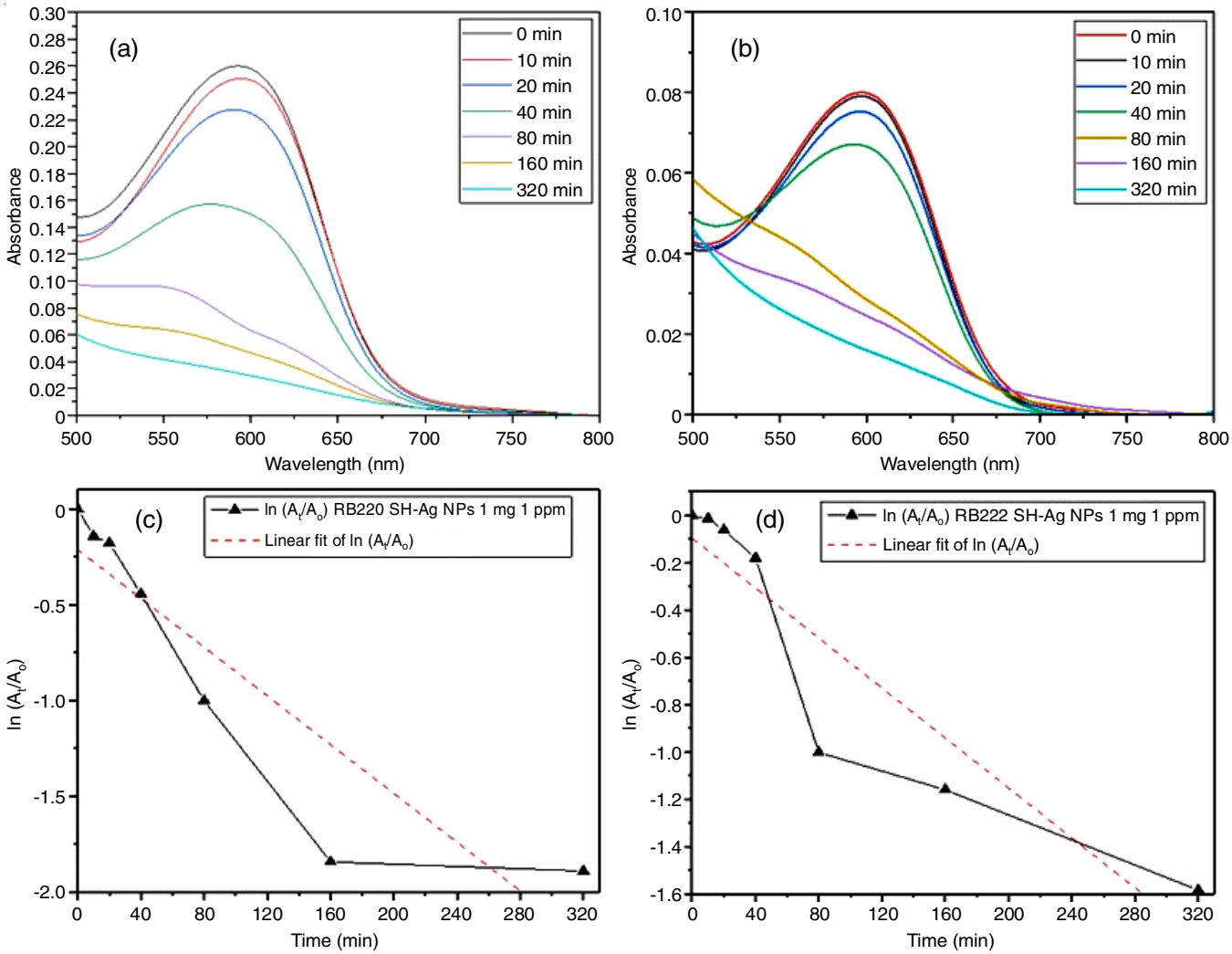

Fig. 6. Photocatalytic degradation of reactive blue 220 (RB-220) dye (a), reactive blue 222A (RB-222A) dye (b) at different time interval and its chemical kinetics plots for RB-220 (c) and RB-222A (d) dyes

These ROS are highly effective oxidizing agents that assist in the breakdown of color molecules. The dye molecules are drawn to the surface of silver nanoparticles by electrostatic interactions and van der Waals forces [17,18]. This approach mainly depends on the ROS-mediated degradation mechanism. Hydroxyl radicals, in particular, induce the chemical reactions within dye molecules to break, eventually leading to degradation. As a result, the original dye molecules are changed into smaller, less complex breakdown products that are frequently colourless or have a lower colour intensity. The proposed mechanism for the degradation of dyes using biosynthesized Ag NPs can be understood from Fig. 7.

Phytotoxicity studies: The toxicity of dyes was evaluated in both untreated and treated samples, and the phytotoxicity results for these dyes are presented in Table-1. It is noted that when *V. radiata* seeds were treated with SH-Ag NPs, the inhibition of germination was significantly reduced. Modi *et al*. [19] demonstrated that Ag NPs are effective in reducing the suppression of seed germination. According to Ozkan *et al.* [20], artemia is a good model for toxicity tests due to its vital role in the aquatic environment. The artemia toxicity experiment indicated that addition of SH-Ag NPs to dyes was extremely effective in reducing the toxic effects of industrial dye pollution in water. According to studies like Ravichandran *et al.* [21], Artemia species are not harmed by Ag NPs, making them a viable choice for cleaning the industrial effluents in aquatic settings. Verma *et al*. [22] demonstrated that the decolorization process decreased the toxicity of reactive blue 4 towards *V. radiata* and *A. salina*. This suggests that the impact of toxicity may differ depending on the specific dye and species involved.

Conclusion

There is a tremendous deal of potential for nanoparticles that have been biosynthesized in an environmental friendly manner to facilitate the degradation of dyes. Such nanoparticles contain various types of biocompatible components and provide a sustainable and effective solution for the dye removal in the wastewater treatment. In this work, a simple and eco-friendly method for synthesizing silver nanoparticles (Ag NPs) from *Strobilanthus hamiltoniana* leaf extract which is rich in phytochemicals and free of toxins was carried out. In UV-vis analysis, SH-Ag NPs had a peak absorbance at 432 nm indicating that

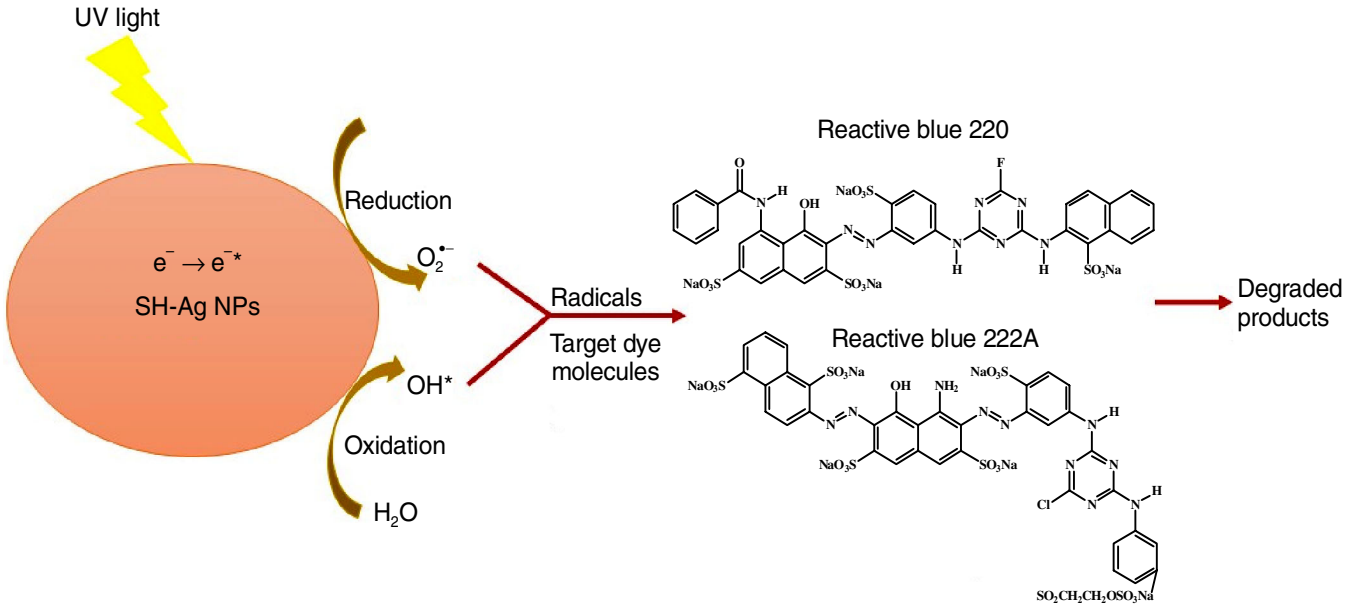

Fig. 7. Proposed mechanism of degradation of reactive blue dyes using biosynthesized silver nanoparticles (SH-Ag NPs)

TABLE-1
PHYTOTOXICITY STUDIES

Characters and treatment	*Vigna radiata* toxicity			Brine shrimp mortality		
	Germination (%)	Average stem toxicity (%)	Average root toxicity (%)	Average initial number of live nauplii	Average number of dead nauplii	Mortality (%)
Distilled water	100	0	0	10.0 ± 0	0.66 ± 0.57	3.33
Negative control ($KMnO_4$ solution)	–	–	–	10.0 ± 0	9.75 ± 0.58	93.33
RB 220	30	51.64 ± 0.57	10.52 ± 0.22	10.0 ± 0	8.66 ± 0.57	66.66
RB 222	39	38.46 ± 0.57	26.31 ± 0.57	10.0 ± 0	8.00 ± 1.00	46.66
SH-Ag NPs	90	9.89 ± 0.57	26.13 ± 1.15	10.0 ± 0	1.60 ± 0.57	16.66
T- RB 220	95	27.47 ± 0	5.26 ± 0.50	10.0 ± 0	1.33 ± 0.57	16.66
T-RB 222	94	14.28 ± 0.0	15.78 ± 0.57	10.0 ± 0	1.00 ± 1.00	10.00

they had an excellent absorption capacity. With an average diameter of 86.46 nm, FESEM analysis verified their primarily spherical form. The crucial role of the functional groups in the synthesis of SH-Ag NPs was highlighted by FTIR analyses. Using biosynthesized Ag NPs, the degradation rates of 88.4% and 79.49% after 320 min was achieved for reactive blue 220 and reactive blue 222A dyes, respectively. Furthermore, a substantial reduction in inhibitory efficacy was also observed when comparing the phytotoxicity in SH-Ag NPs-treated dye solutions to dye effluents, emphasizing the potential environmental advantages of this treatment.

CONFLICT OF INTEREST

The authors declare that there is no conflict of interests regarding the publication of this article.

REFERENCES

1. R. Al-Tohamy, S.S. Ali, F. Li, K.M. Okasha, Y.A.-G. Mahmoud, T. Elsamahy, H. Jiao, Y. Fu and J. Sun, *Ecotoxicol. Environ. Saf.*, **231**, 113160 (2022); https://doi.org/10.1016/j.ecoenv.2021.113160
2. B. Lellis, C.Z. Fávaro-Polonio, J.A. Pamphile and J.C. Polonio, *Biotechnol. Res. Innov.*, **3**, 275 (2019); https://doi.org/10.1016/j.biori.2019.09.001
3. A.K.D. Alsukaibi, *Processes*, **10**, 1968 (2022); https://doi.org/10.3390/pr10101968
4. S. Samsami, M. Mohamadizaniani, M.-H. Sarrafzadeh, E.R. Rene and M. Firoozbahr, *Process Saf. Environ. Prot.*, **143**, 138 (2020); https://doi.org/10.1016/j.psep.2020.05.034
5. M.S. Samuel, M. Ravikumar, A. John J., E. Selvarajan, H. Patel, P.S. Chander, J. Soundarya, S. Vuppala, R. Balaji and N. Chandrasekar, *Catalysts*, **12**, 459 (2022); https://doi.org/10.3390/catal12050459
6. K. Sharma, S. Guleria, K.H. Salaria, A. Majeed, N. Sharma, K.D. Pawar, V.K. Thakur and V.K. Gupta, *Ind. Crops Prod.*, **202**, 116951 (2023); https://doi.org/10.1016/j.indcrop.2023.116951
7. V. Katheresan, J. Kansedo and S.Y. Lau, *J. Environ. Chem. Eng.*, **6**, 4676 (2018); https://doi.org/10.1016/j.jece.2018.06.060
8. A.A. Baby and K.R. Raphael, *Asian J. Pharm. Clin. Res.*, **11**, 256 (2018); https://doi.org/10.22159/ajpcr.2018.v11i11.20081
9. S.D. Wangkheirakpam, W.R. Devi, C.B. Singh and W.S. Laitonjam, *J. Adv. Sci.*, **8**, 1523 (2016); https://doi.org/10.24297/jac.v8i1.4033
10. R.S. Dharshini, M. Poonkothai, P. Srinivasan, R. Mythili, A. Syed, A.M. Elgorban, T. Selvankumar and W. Kim, *Appl. Nanosci.*, **13**, 2527 (2023); https://doi.org/10.1007/s13204-021-02002-3

11. M. Bilal, M. Iqbal, H. Hu and X. Zhang, *Water Sci. Technol.*, **73**, 2332 (2016); https://doi.org/10.2166/wst.2016.082
12. B. Kumar, K. Smita, L. Cumbal and A. Debut, *Saudi J. Biol. Sci.*, **24**, 45 (2017); https://doi.org/10.1016/j.sjbs.2015.09.006
13. N. Liaqat, N. Jahan, Khalil-ur-Rahman, T. Anwar and H. Qureshi, *Front. Chem.*, **10**, 952006 (2022); https://doi.org/10.3389/fchem.2022.952006
14. S.K. Balavandy, K. Shameli, D.R.B.A. Biak and Z.Z. Abidin, *Chem. Cent. J.*, **8**, 11 (2014); https://doi.org/10.1186/1752-153X-8-11
15. M.I. Skiba, V.I. Vorobyova, A. Pivovarov and N.P. Makarshenko, *J. Nanomater.*, **2020**, 3051308 (2020); https://doi.org/10.1155/2020/3051308
16. A.T. Miah, B. Malakar and P. Saikia, *Catal. Lett.*, **146**, 291 (2016); https://doi.org/10.1007/s10562-015-1644-y
17. G. Palani, H. Trilaksana, R.M. Sujatha, K. Kannan, S. Rajendran, K. Korniejenko, M. Nykiel and M. Uthayakumar, *Molecules*, **28**, 3520 (2023); https://doi.org/10.3390/molecules28083520
18. H. Kumari, Sonia, Suman, R. Ranga, S. Chahal, S. Devi, S. Sharma, S. Kumar, P. Kumar, S. Kumar, A. Kumar and R. Parmar, *Water Air Soil Pollut.*, **234**, 349 (2023); https://doi.org/10.1007/s11270-023-06359-9
19. S. Modi, V.K. Yadav, N. Choudhary, A.M. Alswieleh, A.K. Sharma, A.K. Bhardwaj, S.H. Khan, K.K. Yadav, J.-K. Cheon and B.-H. Jeon, *Materials*, **15**, 2393 (2022); https://doi.org/10.3390/ma15072393
20. Y. Ozkan, I. Altinok, H. Ilhan and M. Sokmen, *Bull. Environ. Contam. Toxicol.*, **96**, 36 (2016); https://doi.org/10.1007/s00128-015-1634-1
21. V. Ravichandran, S. Sumitha, C.Y. Ning, O.Y. Xian, U. Kiew Yu, N. Paliwal, S.A.A. Shah and M. Tripathy, *Green Chem. Lett. Rev.*, **13**, 102 (2020); https://doi.org/10.1080/17518253.2020.1738562
22. A.K. Verma, C. Raghukumar, R.R. Parvatkar and C.G. Naik, *Water Air Soil Pollut.*, **223**, 3499 (2012); https://doi.org/10.1007/s11270-012-1127-3